RSC Advances

ROYAL SOCIETY OF CHEMISTRY

www.rsc.org/advances

Candida rugosa lipase immobilization on magnetic silica aerogel nanodispersion

Leila Amirkhani[1], Jafarsadegh Moghaddas[1*] and Hoda Jafarizadeh-Malmiri[2]

[1] Transport Phenomena Research Center (TPRC), Faculty of Chemical Engineering, Sahand University of Technology, 51335-1996 Sahand, Tabriz, Iran

[2] Faculty of Chemical Engineering, Sahand University of Technology, 51335-1996 Sahand, Tabriz, Iran

*Address for correspondence: Jafarsadegh Moghaddas, PhD, Professor

Tel: +98 4133459155, *Fax*: +98411-3444355

E-mail: jafar.moghaddas@sut.ac.ir

Abstract

In this work, the magnetic silica aerogel support was prepared by iron oxide nanoparticles and sodium silicate precursors in a sol-gel process followed by chemical surface modification and ambient pressure drying. Immersion of the silica gels in nanoparticles alcoholic solution was used to synthesis nanocomposites. Characterizations of synthesized samples by BET, FE-SEM, TEM, FTIR, XRD and VSM showed the homogeneous surface morphology, the large surface area (520 m^2/g), mesoporosity, superhydrophobicity and ferromagnetic property which are the attractive properties of magnetic aerogels as supports for lipase immobilization. The synthesized nanocomposites were dispersed in alcoholic solution and used to immobilize *Candida rugosa* lipase by adsorption method. The influence of the sonication amplitude and time in lipase immobilization yield and activity were studied using response surface methodology (RSM). Comparison between the performance dispersed and non-dispersed supports revealed the positive effect of dispersion process on immobilization yield and enzyme activity. The success of immobilization was confirmed by confocal laser scanning microscope (CLSM), proving that enzyme is well distributed in the dispersed magnetic silica aerogel. A comparative study between free and immobilized lipase on dispersed support, was conducted in terms of pH, temperature, thermal stability and the kinetic parameters. Maximum adsorption capacity of lipase was estimated as 81.9 mg g^{-1} based on Langmuir isotherm.

Keywords: Magnetic silica aerogel; Dispersion; Response surface methodology (RSM); Ambient pressure drying; Immobilization; *Candida rugosa* lipase

1. Introduction

Enzymes are biological catalysts that promote the transformation of chemical species in living systems. They catalyze a multitude of different reactions occurring in biological cells under mild conditions [1, 2]. Lipases (triacylglycerol ester hydrolases, EC 3.1.1.3) has the ability to catalyze a number of reactions making it a unique industrial biocatalyst in chemistry, food, pharmaceutical, agrochemical and biotechnology. It is successfully utilized in a variety of hydrolysis and esterification reactions [3, 4]. The application of lipases due to their short lifetimes, unstable structure and extensive separation costs are limited [5]. Biocatalytic process economics can be enhanced by enzyme reuse and the improvement in enzyme stability afforded by immobilization [6]. Therefore, significant efforts have been made on the preparation of lipases in immobilized forms, which involves a variety of new support materials and immobilization techniques [7]. Enzyme immobilization represents the attachment or incorporation of enzyme molecules onto or into large structures, via binding to a support, cross-linking and encapsulation [8]. Nanostructured biocatalysts such as enzyme nanoparticles [9, 10], enzyme nanogels [11], flower-like enzyme-inorganic hybrid crystals [12, 13], enzyme-metal-organic framework hybrid composites [14-16] and enzyme–polymer conjugates [17-20] have been demonstrated as effective ways to re-engineer enzyme catalysts for improved activity and stability in both aqueous and non-aqueous media [20, 21]. In recent years, magnetic zero-dimensional nanoparticles especially magnetite (Fe_3O_4) have been proved as an important and efficient support for the preparation of immobilized enzyme. But applications of these fine particles usually are difficult because of their tending to aggregation and chemically active natures [3, 22]. One method to solve these problems is coating nanoparticles with inorganic layers such as carbon and silica [23]. Continuous matrix such as silica aerogel can be used to

disperse iron nanoparticles [24, 25]. Silica aerogels and their composites has recently attracted so much considerations because of their unusual properties such as very low density, high porosity, high specific surface area, low dielectric constant and excellent heat insulation value [26, 27]. These structures have been used as supports for enzyme immobilization, using adsorption [28, 29] and encapsulation [30-32] methods.

It has previously been shown that the pore size is critical both for the immobilization yield and for the enzymatic activity; however, less focus has been given to the influence of the particle size. Gustafsson et al. were synthesized three types of discrete mesoporous silica particles with varying particle morphology and particle size and immobilized lipase from *M. miehei* (MML) and *R. oryzae* (ROL) into their pores. They found that the specific activity was clearly affected by the particle size and morphology, but the loading did not differ significantly [33]. In the previous works of enzyme immobilization on silica aerogels by adsorption method, this factor was not investigated.

In this work magnetic Fe_3O_4-silica aerogel were synthesized by simple ambient pressure drying method and water glass as a cheap precursor by soaking the alcogels in iron oxide nanoparticles suspension. The synthesized nanocomposites were dispersed in alcoholic solution and used as supports in immobilization of *Candida rugosa* lipase. Dispersion parameters can be changed the particle size distribution of supports, and thus enzyme immobilization yield and activity. The main objective of this research is to evaluate the effect of dispersion parameters of magnetic silica aerogel supports on immobilization yield and specific activity of *Candida rugosa* lipase. Magnetic properties of the supports provide the separation of them from reaction media through a simple and inexpensive process.

2. Experimental

2.1. Materials

Lipase from *Candida rugosa* (type VII) was purchased from Sigma Aldrich (Saint Louis, MO, USA). Olive oil with high purity was purchased from a local market. Iron oxide nanoparticles were prepared from US Research Nanomaterials Company (Fe_3O_4, high purity, 99.5+%, 15-20 nm). All the other chemicals used were of analytical grade.

2.2. Preparation of magnetic silica aerogel

In first step 1.35 sp. gr. sodium silicate solution was diluted to 1.07 sp. gr. solution with deionized water. Removal of unwanted Na^+ ions from the water-glass solution was carried out by mixing the diluted water-glass solution with the ion exchange resin in equal volume proportion. After formation of silicic acid with pH around 2, ammonium hydroxide solution (1.0 M) was added to raise its pH to 4 for gelation. The obtained silica sol was transferred to the Teflon vessels immediately and a hydrogel formed. The gel, was kept in the oven in 50°C for 180 min to strengthen the silica network. After aging, in order to exchange the pore water, the hydrogels were immersed in isopropyl alcohol at 50°C for 18 h. After pore water exchange with isopropyl alcohol, the obtained alcogel was immersed in isopropyl alcoholic solution of iron oxide nanoparticles at 50°C for 2 days. For preparation alcoholic solution of iron oxide nanoparticles, 0.5 g iron oxide nanoparticles were dispersed in 20 ml isopropyl alcohol. After impregnation, the excess iron oxide solution was discharged. The obtained composite gel was washed three times with isopropyl alcohol and the impregnated wet gels were immersed in Hexane for 24 h to exchange the pore solution. Then the wet gels were immersed in HMDZ/n-hexane (1:4 v/v)

solutions for 12 h at 50°C in order to modify the surface. In final step, the modified gels were dried at room temperature for 24 h and then at 50, 80 and 120°C for 2 h, respectively [34].

2.3. Immobilization of lipase

In this work hydrophobic magnetic silica aerogel nanodispersion was used to immobilize *Candida rugosa* lipase. The supports (0.1 g) were dispersed in ethanol solution (37, %v/v) using a tip sonicator (Bandelin, Sonopuls 3100). Sonication was carried out using a tip with a diameter of 3 mm (MS 73, Bandelin GmbH), which can transducer a maximum power of 100W at a frequency of 20 kHz. The tip was immersed into the solution to a depth of about 10 mm. An ice-water bath was used to prevent alcohol solution boiling and evaporation. Dispersion was done at sonication amplitude ranging from 25 to 45% with varying sonication time (3-9 min) according to the experimental design. In next step for lipase immobilization, the enzyme solution was added to magnetic silica aerogel nanodispersion and mixture was stirred for 90 min at ambient temperature to complete adsorption presses. To prepare enzyme solutions, the appropriate amount of enzyme powder was added to 20ml phosphate buffer solution (0.2 M, pH 7.0). The ratio of enzyme to support was considered 0.45 (w/w). After that, the suspension was filtrated and the supports with immobilized lipase were separated, washed with phosphate buffer to remove the unabsorbed enzyme and dried in the air. The filtrate and washing solutions were collected for protein determination [35]. Fig. 1 shows schematic representation of the synthetic procedure of biocatalyst.

In order to study the effect of dispersion process on lipase activity and immobilization yield, non-dispersed supports also were used after pre-wetting in 5 ml of ethanol solution (37, %v/v) in a closed conical flask for 3 hours. Next, the alcohol solution was discharged and the pre-wetted

supports were suspended into enzyme solution. The other steps were done according above procedure.

2.4. Characterization

Atomic absorption spectrometry (AAS, Analytic Jena novAA 300, Germany) was used for obtaining the Fe contents in the nanocomposites. The bulk density of the nanocomposites was calculated using a microbalance scale (10^{-5} g precision, Mettler Toledo, AT261 DeltaRange, Greifensee, Switzerland) and coulisse. The BET surface area and pore size distribution of the samples were measured using the amount of N_2 gas adsorbed at various partial pressures (BET, Belsorp mini II, Japan and Quantachrome Instruments CHEMBET - 3000, USA). The pore structure and particle morphology were characterized by transmission electron microscopy, TEM, (Philips EM208, Eindhoven, Netherlands) and field emission scanning electron microscopy (MIRA3 FE-SEM, Tescan, Czech). Organic and inorganic bonds present in the composite samples were studied by Fourier transform infrared spectroscopy (FTIR) using an IR spectrophotometer (PU 9800, from Philips, the Netherlands). X-ray diffraction (XRD) measurements were performed at room temperature with a Bruker D8, Germany, advance X-ray diffractometer using Cu Kα radiation. Magnetic properties of samples were studied by a vibrating sample magnetometer (VSM, Daghigh Meghnatis Kashan Co.) at room temperature.

Dynamic light scattering (DLS) was used to measure the particle size distributions of dispersed supports (Nano Series, Malvern Instrument, UK). To confirm that the lipase was successfully immobilized on magnetic silica aerogel, lipase molecules were labeled by fluorescein isothiocyanate (FITC) before immobilization and the image of confocal laser scanning

microscopy (CLSM) was taken using a Nikon PCM 2000 confocal microscope (Nikon Instech Co., Kanagawa, Japan) and the excitation wavelength was chosen to be 495 nm.

2.5. Lipase activity assay

Immobilized lipase activity was measured using the method based on olive oil hydrolysis. In this method, 100 ml olive oil emulsion was prepared by mixing 50 ml olive oil and 50 ml gum arabic solution (7% w/v). 3.0 ml phosphate buffer (0.2 M, pH 7.0) and 1ml free lipase (1 mg) or immobilized lipase (60 mg) were mixed at 37˚C using shaking in water bath at 100 rpm. After increasing the temperature of the enzyme solutions to 37˚C, 5.0 ml substrate (olive oil) emulsion was added to it and after 15 min the reaction was stopped by the addition of 20 ml of acetone-ethanol solution (1:1 v/v). The liberated fatty acid in the medium was determined by titration with NaOH solution (0.05 N). One lipase unit corresponded to the release of 1 μmol of fatty acid per minute under the assay conditions. The specific activity is the number of lipase units per mg-protein [36, 37].

Protein content before and after immobilization was determined by the Lowry method using bovine serum albumin as the standard [38].

Immobilization yield percentage (%) was calculated as in the following equation (1):

$$\% \text{ Immobilization yield} = \text{Amount of protein loaded} / \text{Amount of protein introduced} \times 100 \quad (1)$$

Where, amount of protein loaded was calculated as the difference between initial protein introduced concentration and concentration of protein in supernatant after immobilization.

2.6. Experimental design, optimization and statistical analysis

A five level central composite design with two factors was employed to determine the effect of dispersion parameters, such as sonication amplitude (x_1) and sonication time (x_2) on lipase activity (Y_1) and immobilization yield (Y_2). Response surface methodology (RSM) was used to evaluate the effects of independent variables on the response variables. Each independent parameter was studied at five different levels, namely, central point (x_1: 35 %, x_2: 6 min), level -1 (x_1: 25 %, x_2: 3 min), level 1 (x_1: 45 %, x_2: 9 min), level -α (x_1: 21 %, x_2: 1.8 min) and level α (x_1: 49 %, x_2: 10.2 min). The independent variables and their levels are shown in Table S1. A second order polynomial equation (2) was used to express the lipase activity and immobilization yield as a function of the studied variables.

$$Y= a_0+a_1x_1+ a_2x_2+a_{11}x_1^2+ a_{22}x_2^2+ a_{12}x_1x_2 \quad (2)$$

Where, Y_i and x_i represent the responses and independent variables, respectively, a_0 is a constant, a_i , a_{ii} and a_{ij} are the linear, quadratic and interaction coefficients, respectively. Adequacy of the models was examined taking into account the coefficient of determination (R^2) and adjusting the coefficient of determination (R^2-adj) besides. To fit the second order polynomial equation, analysis of variance (ANOVA) was used [39]. A small P-value ($p< 0.05$) represents significance of each term in the models. For graphical explanation of the independent variable interactions, three dimensional surface plots of the model were used. This is useful to visualize the relationship between the response and the experimental levels of each factor. Numerical optimization was performed by the response optimizer for determining the exact optimum amount of independent variables leading to maximum enzyme activity and immobilization yield. The experimental design, data analysis and optimization procedure were performed using the Design Expert version7 statistical software (Stat-Ease Inc., NY, USA).

2.7. Physico-chemical properties of free and immobilized lipase

The effect of pH on activity of the free and immobilized lipase was assayed in phosphate buffer (0.2 M) of pH ranging from 6 to 8.5 by using the standard activity assay procedure mentioned above.

The optimal temperature on the activities of the free and immobilized lipase was investigated in the temperature range 30 to 60˚C under the assay conditions.

In order to test the thermal stability, the residual activity of the free and immobilized lipases was measured after being incubated in phosphate buffer (3 ml, 0.2 M, pH 7.0) at 60˚C for various periods of time for 0 min, 30 min, 60 min, 90 min and 120 min, respectively. After the enzyme was cooled to room temperature the activity was determined under standard conditions (pH 7.0, 37˚C) as described above.

The kinetic parameters of the Michaelis-Menten equation (3) for the free and immobilized lipases were determined by measuring the initial rates of olive oil hydrolysis.

$$v = \frac{v_{\max} S}{K_m + S} \tag{3}$$

Where v_{max} is the highest possible specific lipase activity (U mg protein^{-1}), and K_m is the Michaelis constant (mM) determined from substrate concentration that gives a specific lipase activity of 1/2 v_{max} [40]. The specific activity of lipase (v) was determined over the olive oil concentration (S) range of 0-63 mM.

To test the reusability of immobilized lipase, the supports were separated from reaction medium by magnetic field. Post-treatment of biocatalysts was done by washing three times with phosphate buffer (0.2 M, pH 7.0) and dried for 1 hour. Recovered immobilized lipase was used

in the next activity assay with fresh substrates. The assay condition was the same as described above.

In this study, the relative activity (%) was defined as the ratio of the maximum activity value of lipase in optimum or initial condition to the residual activity of each sample.

3. Results and discussions

3.1. Characterization of synthesized magnetic silica aerogel

In synthesis iron oxide- silica aerogel nanocomposites by soaking method, the total iron oxide nanoparticles was not impregnated onto gel, and also a part of doped iron oxide was lost during the subsequent solvent exchange steps. Thus the atomic adsorption spectroscopy was used to determine the residual final amount of iron in the prepared supports. AAS analysis showed the presence of 3.71% wt of iron in the prepared nanocomposites.

Density and specific surface area of the prepared composite was 0.34 g/cm^3 and 520 m^2/g, respectively. Fig. 2(a) shows the nitrogen adsorption- desorption isotherm of magnetic silica aerogel. The biocatalyst exhibited type IV isotherm which was given by mesoporous materials and a superposition of H1 hysteresis loop according to IUPAC classification, which suggests the presence of narrow distribution of cylindrical-like pores. The pore size distributions of samples determined by BJH method are given in Fig. 2(b). The pore size is between 1 and 11 nm with a relatively sharp peak between 2 and 3 nm suggesting uniform pore size. This mesoporous structure provides enough space for *C. rugosa* lipase immobilization. Also due to high specific surface area and large amount of nanopores, this carrier can facilitate the uptake of substrate and thus increase the immobilization yield and apparent activity of immobilized lipase [41].

Fig. 3 gives the XRD patterns of the iron oxide and prepared iron oxide-silica aerogel nanocomposites. The pattern for nanocomposite had three characteristic peaks at 30.3˚ (220), 35.7˚ (311) and 62.7˚ (440) which was consistent with the standard pattern of Fe_3O_4 (00-019-0629). The broad peak between 20 and 30 degree in pattern of nanocomposite, was due to amorphous silica. This proved the existence of both amorphous silica and magnetite in nanocomposite structure.

Crystallite size (D) is calculated using the Debye-Scherer's formula [42]:

$$D = \frac{k\lambda}{\beta \cos\theta} \quad (4)$$

Where β is the full width at half maximum (FWHM) of the corresponding XRD peak, k is a constant (~1), λ is X-ray wavelength and θ is the Bragg angle. Using Scherrer equation the mean crystallite size of FeO was obtained as 42 nm and 21 nm for magnetite and magnetite- silica aerogel nanocomposites. These results revealed nano crystallite size of structures.

Fig. 4 shows the FTIR investigation of the sample. In this figure the absorption peak at 585cm^{-1} is the characteristic absorption of a Fe-O bond that confirm the presence of iron oxide particles in the samples [43]. The major peaks at around 3500 and 1650 cm^{-1} are attributed to O-H bonding. The peaks at around 2900 and 1450 cm^{-1} indicates to C-H bonds. The peaks at around 1092 and 854 cm^{-1} show asymmetric and symmetric of SiO_2 respectively. The strong peak in 469cm^{-1} are attributed to O-Si-O bond [44].

Field emission scanning electron micrograph (FESEM) and transmission electron microscopy (TEM) of nanocomposites are shown in Fig. 5. It can be seen that the microstructure of composite was a three-dimensional nanoporous structure composed of nanoparticles with good uniformity. The figure also showed that the particles and the pores size were less than 50 nm in

agreement with XRD results. The TEM image showed that iron oxide nanoparticles were surrounded by porous silica aerogel matrix.

Magnetization curve of synthesized sample in room temperature (298K) was obtained by the use of vibrating sample magnetometer (VSM) with maximum magnetic field of 10 kOe (Fig. S1). The results indicated that the silica aerogel-iron oxide nanocomposite exhibited ferromagnetic behavior and the value of saturation magnetization (Ms) was 6.16 emu/g. The M_S value of pure magnetite nanoparticles was 60.45 emu/g. After silica coating, the Ms value of magnetic silica aerogel was decreased. One of the important reasons is that the non-magnetic silica aerogel layer, influences the uniformity or magnitude of magnetization due to quenching of surface moments decreases surface moments. On the other hand in nanocomposite structure there is a little amount of ferromagnetic nanoparticles per unit weight [45].

3.2. Optimization of dispersion parameters

Ambient pressure-dried magnetic silica aerogels are prepared from hydrocarbon exchanged gels and require the use of silylating agents to minimize forces exerted onto the gels during drying and to prevent structural collapse. Hexamethyldisilazane (HMDZ), provides proper number of non-polar groups ($-CH_3$) for the surface modification of the gel through the $O-Si-CH_3$ groups. Thus the resulting aerogel in this method have hydrophobic surfaces [46].

The hydrophobic/hydrophilic nature of the carriers surrounding the enzyme molecules can affect the interfacial activation of them and the distribution of substrates between bulk solvent and protein surface [41, 47]. It has been shown that lipases prefer to adsorb on hydrophobic supports. Most types of lipase have a peptide ‘lid’ covering the active site. The lid shifts to an ‘open’ conformation in hydrophobic environments. Thus with immobilization of lipase in hydrophobic

carriers, these enzymes can be kept in open and active form [41]. On the other hand the superhydrophobic nature of supports don't allow free enzyme to penetrate in pores. It seems that with a considerable decrease in interfacial tension, the penetration of lipase into inner surface of the pores is possible. In fact, by pre-wetting the supports with alcohol the lipase penetrates easily into the supports and, after drying, when the alcohol leave the pores, lipase molecules present in active form in hydrophobic media and act at their highest capacity. On the other hand, the treatment supports with some polar solvents on immobilized lipases, can increase their activity and stability. Activity enhancement is explained by opening the lid of the enzyme that is caused by ethanol solution [48, 49].

Internal diffusion within carriers can restrict the apparent activity of immobilized enzyme. A smaller size of carriers often gives a higher catalytic efficiency due to the reduced internal diffusion resistance [41]. With dispersion and ultrasounding, magnetic silica aerogels change to nanoporous segments, which save their initial properties. Nanodispersions without stabilizers were stable for several hours to a few days and then agglomeration occurred causing their deposition [50]. Highly dispersed carriers can display greatly enhanced enzyme activity. But separation and recovering of very small supports after the reaction is difficult [47].

Thus with dispersion magnetic silica aerogel in alcoholic solution and optimization the dispersion parameters, in addition to pre-wet the supports, the appropriate size for maximize the activity and immobilization yield can be find.

3.2.1. Fitting the response surface models

The activity and immobilization yield of *Candida rugosa* lipase on nanodispersed magnetic silica aerogel obtained from experimental runs in different dispersion conditions are shown in Table 1.

Equation 2 was used to fit the data. The estimated regression coefficients for final reduced models as well as the corresponding significance of regressions were given in Table 2. It should be considered that lower p value and higher F ratio corresponds to higher significance of a term on studied response variations. P value less than 0.05 for a factor indicates that its effect is significant. The reduced models were obtained after removing the non-significant terms. The results indicated that the coefficient of determination (R^2) of model for the response of the enzyme activity was 0.9936 and the R^2 value for the response of immobilization yield was 0.9878. The obtained high R^2 values confirmed the suitability of the suggested models. Furthermore, the attained non-significant lack of fits and high F values for the suggested models ensured the models were significant (Table 2).

3.2.2. Analysis of response surfaces

As shown in Table 1, enzyme specific activity and immobilization yield varied from 13.6 to 17.8 U/mg-protein and 70.1 to 79.8%, respectively. As clearly observed in Table 2, the linear and quadratic terms of all independent variables had significant ($p<0.05$) effects on enzyme activity and immobilization yield. The results indicated that amplitude and sonication time had more significant effects on both responces, respectively, due to their high F ratio values. The resulted regression cofficients showed that, all the main terms had a positive effect on enzyme activity and immobilization yield. It means that at low amplitude and sonication time, the enzyme activity and immobilization yield increased by an increase in all the mentioned independent variables and vice versa. The opposite results were obtained for effects of all the independent variables at their high level on the activity of immobilized enzyme and immobilization yield (Table 2).

As clearly observed in Table 2, the interaction of sonication amplitude and time had non-significant effect on immobilization yield. While this interaction had significant effect on activity of immobilized lipase. Fig. 6 shows the interactive effect of parameters on lipase activity. As indicated in this figure, at constant level of each parameter by increasing the other parameter, enzyme activity was increased at first to reach its maximum amount and then was decreased. The results indicated that maximum enzyme activity (17.9 U/mg-protein) was obtained at 32% amplitude and middle time (5.5 min). Increase in sonication amplitude would increase the ultrasonic radiation forces and led to a reduction in the particle size of the support. It was attributed to higher shear force or disruption mechanism applied, which breaks magnetic silica aerogel in to a smaller size. Also higher sonication time favored the formation of nanodispersed solution with smaller particle size. It was due to the longer duration for the action of ultrasonic radiation forces to disperse the magnetic silica aerogel into smaller sizes [51]. A probable explanation to why the lipases have higher activity in smaller particles compared to the larger particles, is that the smaller particles have shorter pores and therefore a larger relative amount of enzyme accessible to the substrate [33].

The pure silica aerogel are very porous and fragile. In magnetic silica aerogels, incorporation of the iron nanoparticles in aerogel pores improved the mechanical properties. In dispersion step with more increasing in sonication time and amplitude, the particles size became smaller and magnetic nanoparticles was emitted from the pores and the composite pores structures were damaged. So immobilization yield and enzyme activity were decreased in high sonication time and amplitude.

3.2.3. Optimization and verification of the dispersion conditions

The amount of sonication time and amplitude would be considered optimum if enzyme activity and immobilization yield attain the largest possible values. Numerical optimization was used to find the exact optimum levels of the studied variables. The optimum sonication conditions were: 36% amplitude and 6.2 min sonication time. The highest specific activity and immobilization yield in these conditions predicted by the equations, were 17.6 U/mg-protein and 79.1% respectively.

The optimal conditions were verified using an experimental test and were in good agreement with the predicted results (Table S2), implying that the models derived from RSM can be used to adequately describe the relationship between the factors and responses in immobilization of *Candida rugosa* lipase in nanodispersed magnetic silica aerogel supports.

3.3. Particle size determination

Sonication time and amplitude were affected directly on particle size of magnetic silica aerogel segments. So after optimization the sonication parameters to maximize enzyme activity and immobilization yield, particle size distribution were determined in optimum sonication condition. Fig. 7 shows the DLS results of dispersed magnetic silica aerogel in alcoholic solution using 36% sonication amplitude and 6.2 min sonication time. As shown in this picture the average size of segments was 1600nm with narrow size distribution.

3.4. Comparison between dispersed and non-dispersed supports

In order to investigate the effect of dispersion process on immobilization yield and enzyme activity, the performance of dispersed and non-dispersed supports at different adsorption time were compared. In the case of dispersed supports, dispersion was done in optimized sonication condition using 36% sonication amplitude and 6.2 min sonication time. Non-dispersed supports

were used after pre-wetting process. Fig. 8 shows the results of this comparison. According to this figure the adsorption process was completed at a reaction time of 90 min for both supports. Immobilization yield and enzyme activity of dispersed support at all times was higher than non-dispersed supports. As shown in the previous section, the dispersed supports have shorter pores and therefore a larger relative amount of enzyme accessible to the substrate. Moreover in non-dispersed supports, the surface pores were saturated with lipase molecules and thus in the inner pores, the adsorption was not happened and immobilization yield in this form was decreased.

These results were confirmed by CLSM images (Fig. 9). This technique has been employed to visualize the distribution of lipase throughout the dispersed and non-dispersed supports as well as to evaluate restrictions to diffusion within them. Because of low magnification of CLSM, 5μm dispersed particles with lipase were employed in the observation. Firstly, as the control image, no fluorescent signal was observed with magnetic silica aerogel without lipase, indicating that any fluorescence would be due to the lipase. As can be seen from Fig. 9(a), in non-dispersed supports the enzyme was not uniformly distributed. There were some dark spaces with no fluorescent signal in these supports due to weak adsorption of lipase on the inner pores. Thus, there is an apparent restriction for diffusional transport into the interior of the non-dispersed supports. But in dispersed supports the lipase distribution was uniform (Fig. 9(b)). So restriction of diffusion was eliminated in these supports by well dispersion.

3.5. Adsorption isotherm of lipase on dispersed support

Adsorption isotherms describe the support capacity and affinity for lipase, while the isotherm shape reflects lipase distribution on the support surface. In order to determine the adsorption capacity of dispersed magnetic silica aerogel for *Candida rugosa* lipase, the Langmuir

adsorption isotherm was employed. Langmuir isotherm corresponds to the immobilization in a monolayer [49].

The Langmuir isotherm is typically represented by equation 5:

$$q = \frac{q_{\max} C_e}{K_d + C_e} \quad (5)$$

Where q is the adsorption capacity defined as the amount of protein adsorbed per unit weight of supports (mg g^{-1}), C_e is the residual amount of protein in unit volume of liquid phase (mg ml^{-1}), q_{max} is the maximum adsorption capacity (mg g^{-1}) and K_d is the Langmuir constant (mg ml^{-1}) related to the energy of adsorption and the affinity between support and enzyme [52].

To determine the adsorption isotherm, different concentrations (0.2-3 mg ml^{-1}) of lipase were incubated with 3 mg ml^{-1} of dispersed supports at ambient temperature and pH of 7 for 90 min to reach equilibrium. Fig. 10 shows that the experimental data of lipase adsorption on dispersed magnetic silica aerogel can be fitted by Langmuir isotherm. The regression coefficient of Langmuir model was 0.97, which implied the formation of a monolayer on the support surface. This result indicates an energetically homogeneous surface where all affinities of the binding sites for the enzyme molecule are identical. According to Langmuir model, the maximum monolayer adsorption capacity of dispersed magnetic silica aerogel (q_{max}) and Langmuir constant (K_d) were 81.9 mg g^{-1} and 4.0 mg ml^{-1} respectively.

3.6. Comparison between properties of free and immobilized lipase

The comparative study on enzymatic properties of both free and immobilized lipase on dispersed support was carried out in terms of pH, temperature, thermal stability and the kinetic parameters.

To study the effect of changing pH on the activity of free and immobilized lipases, pH values from 6 to 8.5 were tested (Fig. S2). The optimum pH for the *Candida rugosa* lipase was shifted

to a more alkaline value after immobilization. The maximum activity of the immobilized lipases was observed at pH 8.0, which was higher than that for the free lipase (pH 7.0). Thus the immobilization of lipase molecules results in improved lipase tolerance to high pH conditions [53].

The dependence of temperature on both free and immobilized lipases is displayed in Fig. S3. From these data, the optimum temperatures for the free lipase and immobilized lipases were 40˚C and 50˚C, respectively. Additionally, the immobilized lipases retained higher activities than free lipase at higher temperatures. This behavior can be attributed to the more rigid structure of the immobilized system.

The rigidity of the immobilized system structure can also explain the higher thermal stability for the immobilized lipase, in contrast to the free enzyme (Fig. S4). Thermal stability of the immobilized lipase in 60˚C was improved toward free lipase. The relative activity was about 60% for immobilized enzyme after 2 h but it reached zero for free lipase in this time [54].

Kinetic studies show that the dependence of dispersed magnetic silica aerogel immobilized lipase activity on substrate (olive oil) concentration can be described by M-M model (Fig. 11). The co-relation coefficients (R^2) of the curve was 0.98. Table 3 shows the kinetics constants of free and immobilized lipase for the substrate olive oil. The v_{max} is intrinsic catalytic character of the enzyme and K_m reflects the affinity between enzyme and substrate [40].

As shown in table 3, v_{max} was decreased upon immobilization from 71.5 U/mg-protein for the free one to 20.4 U/mg-protein for immobilized lipase. These results show that immobilization had an effect on the enzyme kinetics and reduced activity was the result of a structural change induced by electrostatic and hydrophobic interactions during the adsorption of a protein [40, 55]. The higher K_m value indicated lower affinity of substrate and enzyme. As shown in table 3 the

affinity of immobilized lipase to its substrate was lower than the free lipase (higher k_m value), probably due to the unfavorable conformational transition in the structure of lipase within the matrix that led to hindered accessibility of the substrate to the active site of the immobilized lipase [41].

Reusability is the most important advantage of an immobilized enzyme compared to the free enzyme. The improved stability and reusability can significantly reduce the cost of enzyme and thus make the industrial application economically feasible [56]. The reusability of immobilized enzyme was studied ten times and the results are shown in Fig. S5. It can be observed that the immobilized lipase shows good stability and retains more than 60% of their initial activity after 10 consecutive reuses.

4. Conclusion

In this study, magnetic silica aerogels were synthesized using sodium silicate precursor and iron oxide nanoparticles by ambient pressure drying method. Characterization of these supports by different methods, revealed mesoporosity, hydrophobicity and ferromagnetic properties of synthesized nanocomposites that are attractive for lipase immobilization. *C. rugosa* lipase was successfully immobilized on dispersed supports by simple physical adsorption. Response surface methodology (RSM) and central composite design (CCD) were employed to optimize the sonication parameters that effect on specific enzyme activity and immobilization yield. Kinetic constants indicated the altered enzyme activity after immobilization. The increased protein rigidity caused a decrease of enzyme activity, but increased its temperature stability and reusability. Magnetic silica aerogel showed a promising future for immobilization enzymes as it

allowed easy immobilization and separation from reaction media through a simple and inexpensive process.

References

1 R. A. Sheldon and S. van Pelt, *Chem. Soc. Rev*., 2013, **42**, 6223-6235.

2 J. M. Guisan, Immobilization of Enzymes and Cells. 2th ed. Totowa, New Jersey: Humana Press. 2006.

3 V. Kumar, F. Jahan, S. Raghuwanshi, R. V. Mahajan and R. Kumar Saxena, *Biotechnol*. *Bioprocess*. *Eng*., 2013, **18**, 787-795.

4 F. Hasan, A. A. Shah and A. Hameed, *Enzyme Microb. Technol*., 2006, **39**, 235-251.

5 H. Jafarizadeh-Malmiri, M. A. Ghaz-Jahanian and A. Berenjian, *Am. J. Biochem. Biotechnol.*, 2012, **8**, 203-219.

6 D. Brady and J. Jordaan, *Biotechnol*. *Lett*., 2009, **31**, 1639-1650.

7 Y. Wu, Y. Wang, G. Luo and Y. Dai, *Bioresour. Technol*., 2009, **100**, 3459-3464.

8 S. A. Ansari and Q. Husain, *Biotechnol*. *Adv*., 2012, **30**, 512-523.

9 J. Ge, J. Lei and R. N. Zare, *Nano Lett*., 2011, **11**, 2551-2554.

10 J. Ge , E. Neofytou, J. Lei, R. E. Beygui and R. N. Zare*, Small*, 2012, **8**, 3573-3578.

11 R. Wang, Y. Zhang, J. Ge and Z. Liu, *RSC Adv*., 2014, **4**, 40301-40304.

12 L. Zhu, L. Gong, Y. Zhang, R. Wang, J. Ge, Z. Liu and R. N. Zare, *Chem*. *Asian J*., 2013, **8**, 2358-2360.

13 J. Ge, J. Lei and R. N. Zare, *Nat*. *Nanotechnol*., 2012, **7**, 428-432.

14 X. Wu, J. Ge, C. Yang, M. Hou and Z. Liu, *Chem*. *Commun*., 2015, **51**, 13408-13411.

15 F. Lyu, Y. Zhang, R. N. Zare, J. Ge and Z. Liu, *Nano Lett*., 2014, **14**, 5761-5765.

16 P. Chulkaivalsucharit, X. Wu and J. Ge, *RSC Adv*., 2015, **5**, 101293-101296.

17 Y. Zhang, Y. Dai, M. Hou, T. Li, J. Ge and Z. Liu, *RSC Adv*., 2013, **3**, 22963-22966.

18 J. Zhu, Y. Zhang, D. Lu, R. N. Zare, J. Ge and Z. Liu, *Chem*. *Commun*., 2013, **49**, 6090-6092.

19 X. Wu, J. Ge, J. Zhu, Y. Zhang, Y. Yong and Z. Liu, *Chem*. *Commun*., 2015, **51**, 9674-9677.

20 M. Hou, R. Wang, X. Wu, Y. Zhang, J. Ge and Z. Liu, *Catal*. *Lett*., 2015, **145**, 1825-1829.

21 Z. Li, Y. Zhang, Y. Su, P. Ouyang, J. Ge and Z. Liu, *Chem*. *Commun*., 2014, **50**, 12465-12468.

22 B. Kalska-Szostko, M. Rogowska, A. Dubis and K. Szymanski, *Appl. Surf. Sci.*, 2012, **258**, 2783-2787.

23 A.-H. Lu, E. L. Salabas and F. Schuth, *Angew. Chem. Int. Ed.*, 2007, **46**, 1222-1244.

24 Ll. Casas, A. Roig, E. Rodríguez, E. Molins, J. Tejada and J. Sort, *J. Non-Cryst. Solids*, 2001, **285**, 37-43.

25 M. B. Fernandez van Raap, F. H. Sanchez, A. G. Leyva, M. L. Japas, E. Cabanillas and H. Troiani, *Physica B*, 2007, **398**, 229-234.

26 F. Schwertfeger, D. Frank and M. Schmidt, *J. Non-Cryst. Solids,* 1998, **225**, 24-29.

27 A. S. Dorcheh and M. H. Abbasi, *J. Mater. Process Technol*, 2008, **199**, 10-26.

28 S. Gao, Y. Wang, W. Wang, G. Luo and Y. Dai, *J. Mol. Catal. B: Enzym*., 2010, **62**, 218-224.

29 N. Kharrat, Y. B. Ali, S. Marzouk, Y.-T. Gargouri and M. Karra-Chaabouni, *Process Biochem*., 2011, **46**, 1083-1089.

30 O. Orçaire, P. Buisson and A. C. Pierre, *J. Mol. Catal. B: Enzym*., 2006, **42**, 106-113.

31 H. El Rassy, S. Maury, P. Buisson and A. C. Pierre, *J. Non-Cryst. Solids*, 2004, **350**, 23-30.

32 A. Pierre and P. Buisson, *J. Mol. Catal. B: Enzym*., 2001, **11**, 639-647.

33 H. Gustafsson, E. M. Johansson, A. Barrabino, M. Odén and K. Holmberg, *Colloid. Surface. B*., 2012, **100**, 22-30.

34 H. Bargozin, L. Amirkhani, J. S. Moghaddas and M. M. Ahadian, *Sci. Iran,* 2010, **17**, 122-132.

35 M.-M. Zheng, Y. Lu, L. Dong, P.-M. Guo, Q.-C. Deng, W.-L. Li, Y.-Q. Feng and F.-H. Huang, *Bioresour. Technol*., 2012, **115**, 141-146.

36 A. Kilinc, M. Teke, S. Onal and A. Telefoncu, *Prep. Biochem. Biotech*., 2006, **36**, 153-163.

37 S. F. Chang, S. W. Chang, Y. H. Yen and C. J. Shieh, *Appl. Clay Sci*., 2007, **37**, 67-73.

38 O. H. Lowry, N. J. Rosebrough, A. L. Farr and R. J. Randall, *J. Biol. Chem*., 1951, **193**, 265-275.

39 N. Anarjan, N. Jaberi, S. Yeganeh-Zare, E. Banafshehchin, A. Rahimirad and H. Jafarizadeh-Malmiri, *J. Am. Oil Chem. Soc.,* 2014, **91**, 1397-1405.

40 L. T. I. Zivkovic, L.S. Zivkovic, B. M. Babic, M. J. Kokunesoski, B. M. Jokic and I. M. Karadzic, *Biochem. Eng. J.*, 2015, **93**, 73-83.

41 Y. Zhang, J. Ge and Z. Liu, *ACS Catal*., 2015, **5**, 4503-4513.

42 H. P. Klug, and L. E. Alexender, *X-ray Diffraction Procedures for Polycrystalline and Amorphous Materials*; New York: Wiley. 1974.

43 K. Khoshnevisan, M. Barkhi, D. Zare, D. Davoodi and M. Tabatabaei, *Synth. React. Inorg. M.*, 2012, **42**, 644-648.

44 R. Al-Oweini and H. El-Rassy, *J. Mol. Struct*., 2009, **919**, 140-145.

45 H. Xu, N. Tong, L. Cui, Y. Lu and H. Gu, *J. Magn. Magn. Mater*., 2007, **311**, 125-130.

46 A. Venkateswara Rao, A. Parvathy Rao, and M. M. Kulkarni, *J. Non-Cryst. Solids*, 2004, **350**, 224-229.

47 J. Ge, C. Yang, J. Zhu, D. Lu and Z. Liu, *Top*. *Catal*., 2012, **55**, 1070-1080.

48 S. Chamorro, J. M. Sánchez-Montero, A. R. Alcántara and J. V. Sinisterra, *Biotechnol. Lett.,* 1998, **20**, 499-505.

49 R. M. Blanco, P. Terreros, N. Munoz and E. Serra, *J. Mol. Catal. B-Enzym*., 2007, **47**, 13-20.

50 H. Bargozin and J. S. Moghaddas, *J. Disper. Sci. Technol*. 2013, **34**, 1130-1138.

51 C. L. Ngan, M. Basri, F. F. Lye, H. R. Fard Masoumi, M. Tripathy, R. Abedi Karjiban and E. Abdul-Malek, *Inter*. *J. Nanomed*., 2014, **9**, 4375-4386.

52 D. S. Rodrigues, G. P. Cavalcante, A. L. O. Ferreira and L. R. B. Gonçalves, *Chem*. *Biochem*. *Eng*. *Q*, 2008, **22**, 125-133.

53 M. Kalantari, M. Kazemeini, F. Tabandeh and A. Arpanaei*, J. Mater. Chem*., 2012, **22**, 8385-8393.

54 J. C. Santos, G. F. M. Nunes, A. B. R. Moreira, V. H. Perez and H. F. d. Castro, *Chem*. *Eng*. *Technol*., 2007, **30**, 1255-1261.

55 D.-T. Tran, C.-L. Chen and J.-S. Chang, *J. Biotechnol*. 2012, **158**, 112-119.

56 X. Wu, M. Hou and J. Ge, *Catal. Sci. Technol*., 2015. **5**, 5077-5085.

Table 1. Two factor central composite design and the experimental and predicted values of responses

Run	Amplitude (%)	Time (min)	Specific activity (U/mg-protein)		Immobilization yield (%)	
			Experimental	Predicted	Experimental	Predicted
1	25	3	16.8	16.68	70.1	70.3
2	45	3	15.3	15.19	76.7	77.06
3	25	9	16.7	16.57	72.5	72.9
4	45	9	14.3	14.18	78.4	78.97
5	21	6	16.32	16.45	70.6	70.3
6	49	6	13.6	13.71	79.8	79.3
7	35	1.8	16.5	16.62	73.5	73.25
8	35	10.2	15.7	15.83	77	76.45
9	35	6	17.8	17.73	78.9	78.72
10	35	6	17.75	17.73	78.6	78.72
11	35	6	17.8	17.73	78.4	78.72
12	35	6	17.7	17.73	78.6	78.72
13	35	6	17.6	17.73	79.1	78.72

Table 2. The significance probability (p value, F ratio) of regression coefficients and Lack-of-fit, regression coefficients, R^2 and R^2 adjusted for the final reduced models

Parameters	Variables	Enzyme activity (Y_1)		Immobilization yield (Y_2)		Regression coefficient		
		F ratio	P value	F ratio	P value		Y_1	Y_2
						a_0	0.87	32.32
Main	x_1	353.53	< 0.0001	332.8	< 0.0001	a_1	0.87	1.72
	x_2	29.33	0.0010	41.9	0.0003	a_2	1.17	3.16
Quadratic	x_1^2	574.50	< 0.0001	109.3	< 0.0001	a_{11}	-0.01	-0.02
	x_2^2	186.27	< 0.0001	106.6	< 0.0001	a_{22}	-0.08	-0.21
Interaction	x_{12}	9.54	0.0176	0.50	0.5019	a_{12}	-0.01	-
Regression		215.91	< 0.0001	113.3	< 0.0001			
Lack-of-fit		5.74	0.0623	6.1	0.0570			
R^2		0.9936		0.9878				
R^2 adjusted		0.9890		0.9791				

Table 3. Comparison of kinetics parameters for free and immobilized lipase

	K_m (mM)	v_{max} (Umg^{-1})
Magnetic silica aerogel	8.9	20.4
Free lipase	3.9	71.5

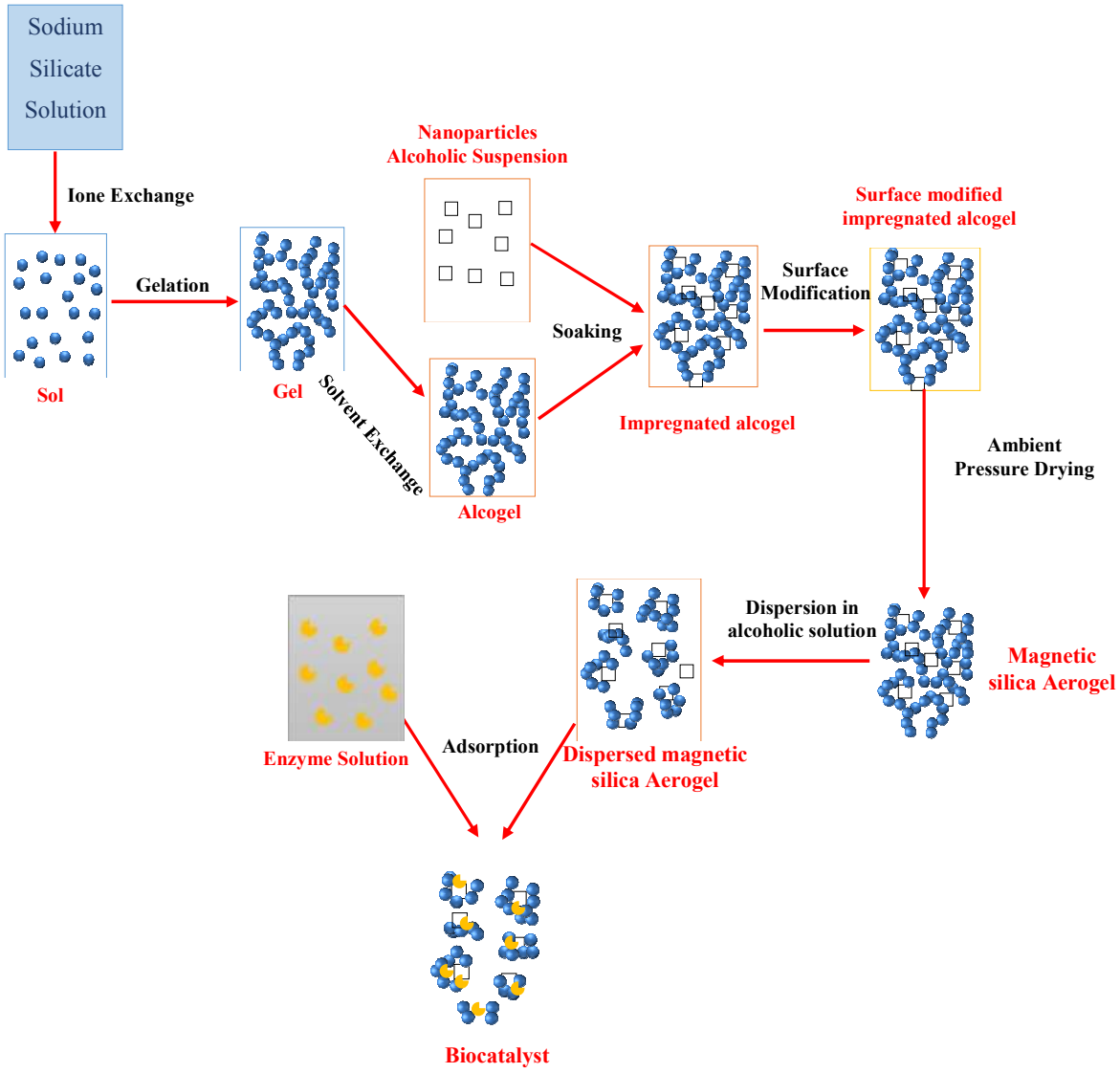

Fig. 1 Schematic representation of the synthetic procedure of biocatalyst

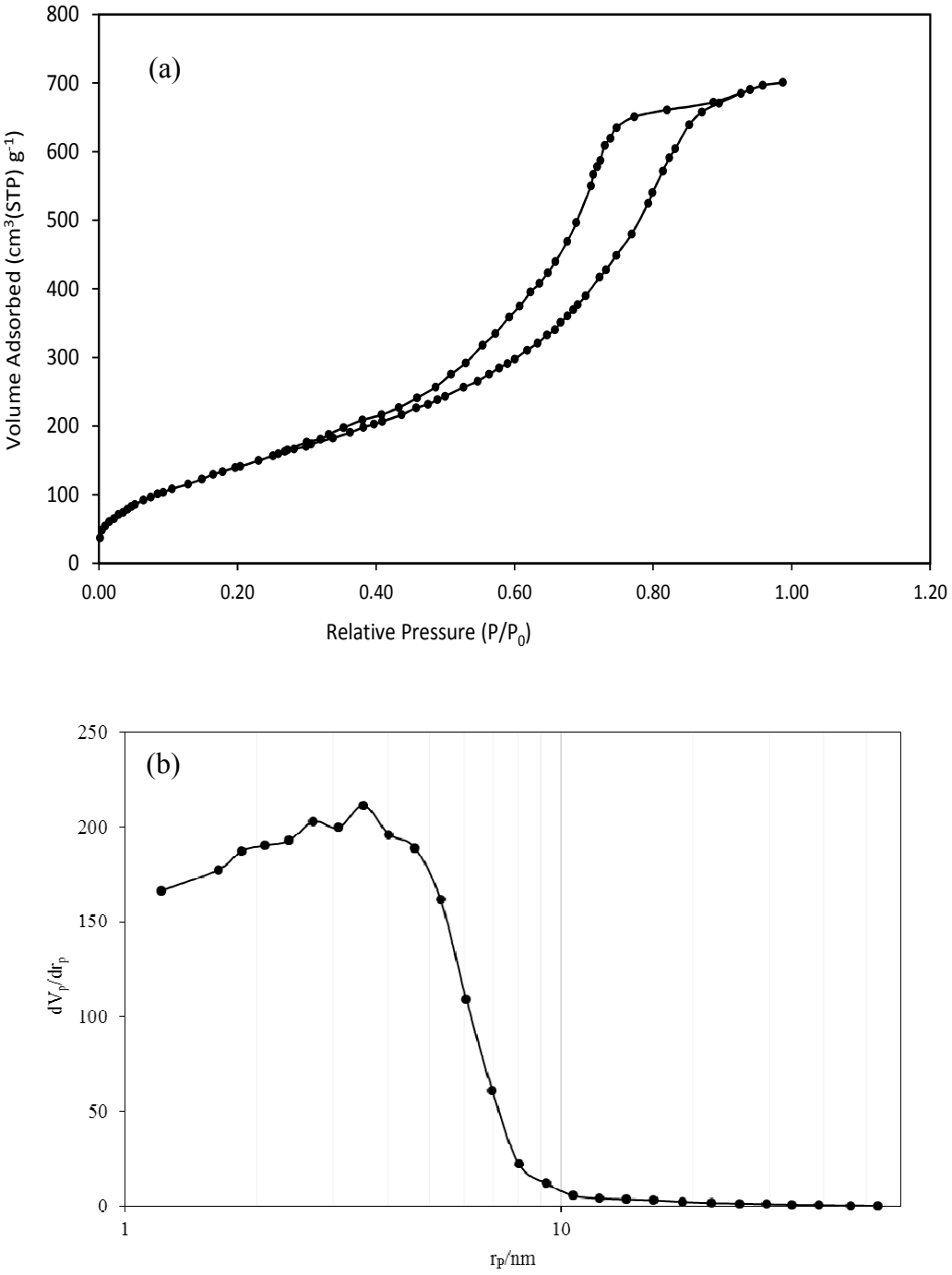

Fig. 2 N_2 adsorption-desorption isotherm (a) and pore size distribution profile (b) of magnetic silica aerogel nanocomposite

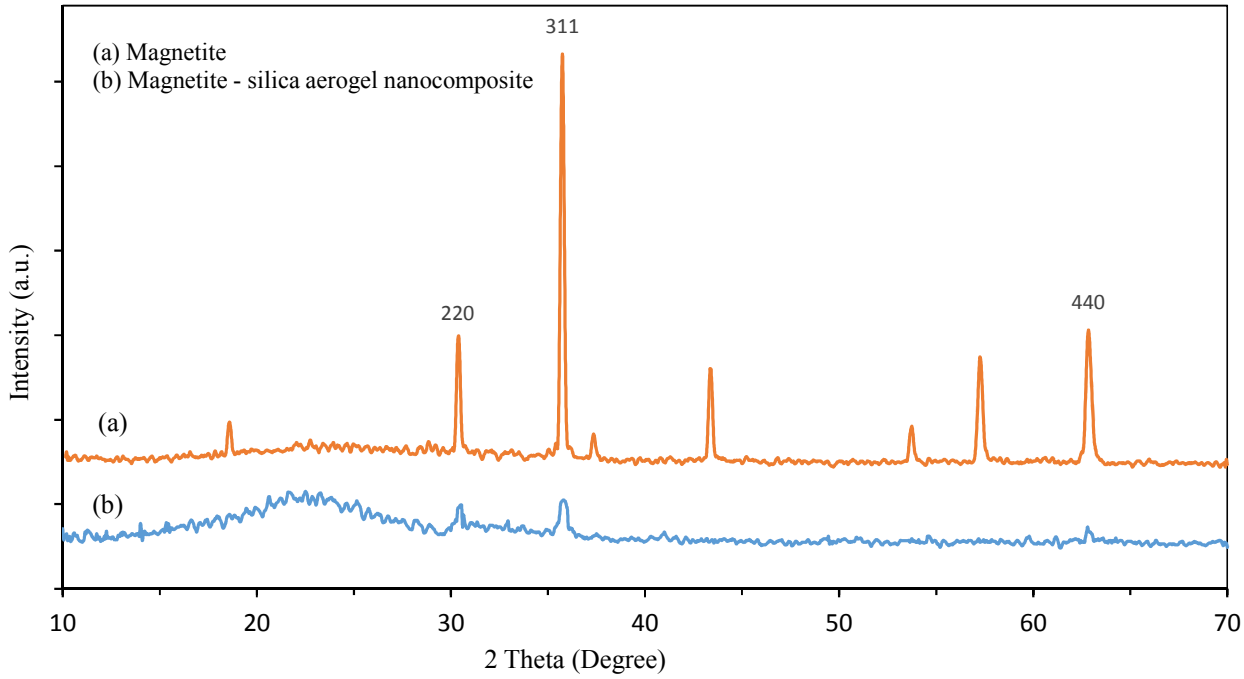

Fig. 3 The XRD pattern of magnetite (a) and magnetite- silica aerogel nanocomposite (b)

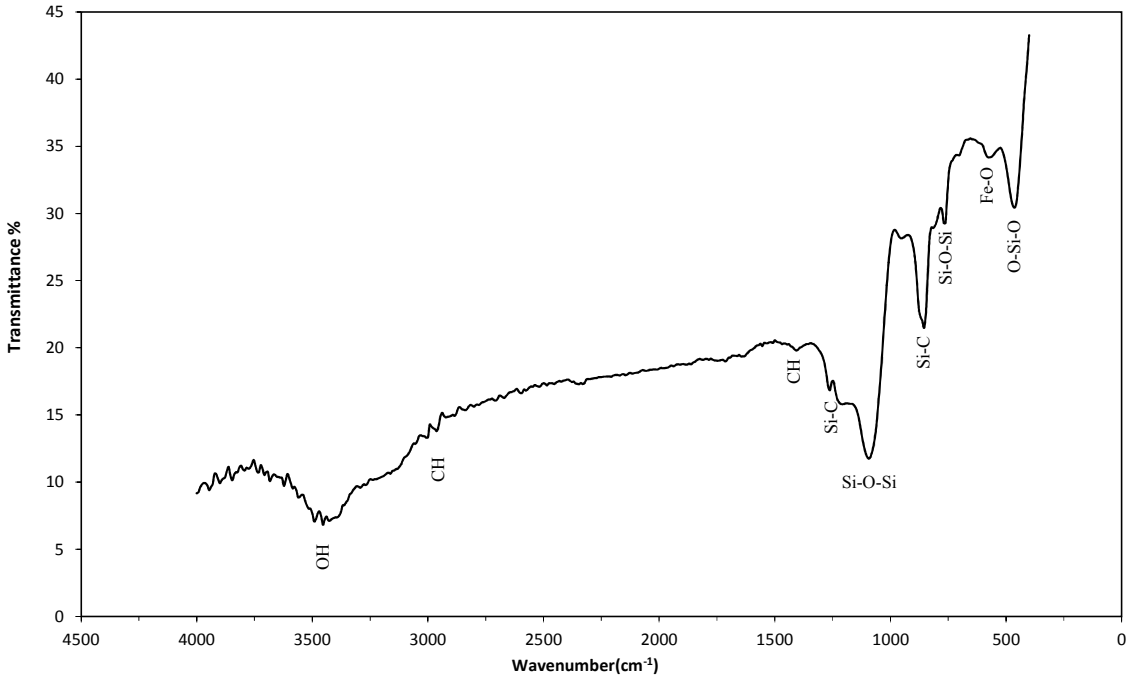

Fig. 4 FT-IR spectrum for magnetite- silica aerogel nanocomposite

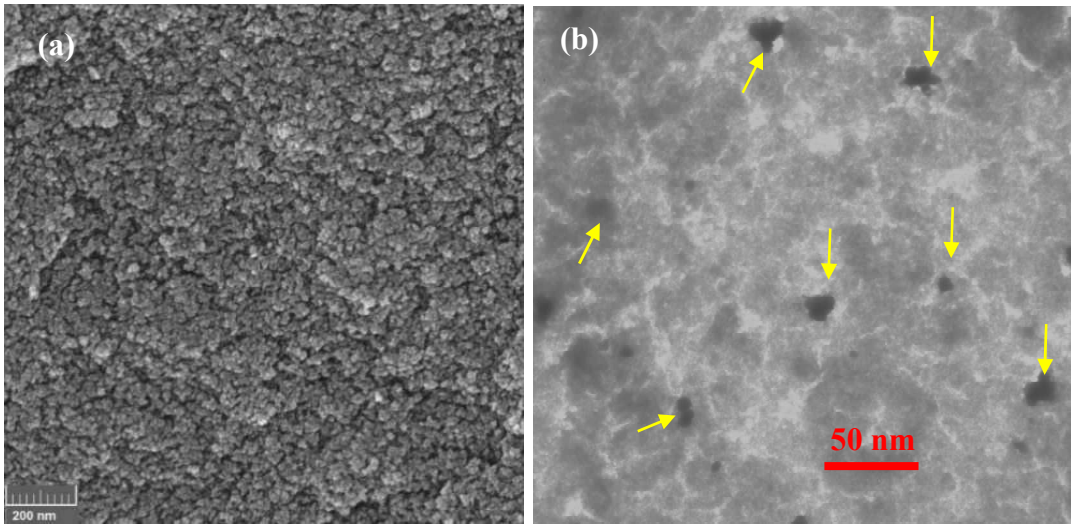

Fig. 5 FESEM (a) and TEM (b) images of magnetite- silica aerogel nanocomposite (Iron oxide nanoparticles were specified with yellow arrows in TEM image)

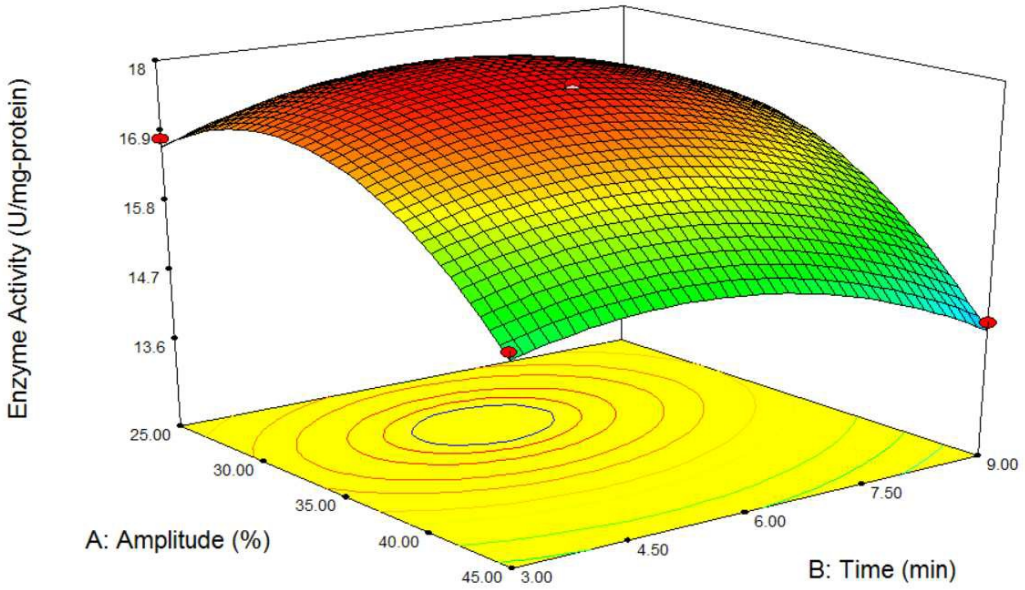

Fig. 6 Response surface plot of specific activity versus sonication amplitude and time

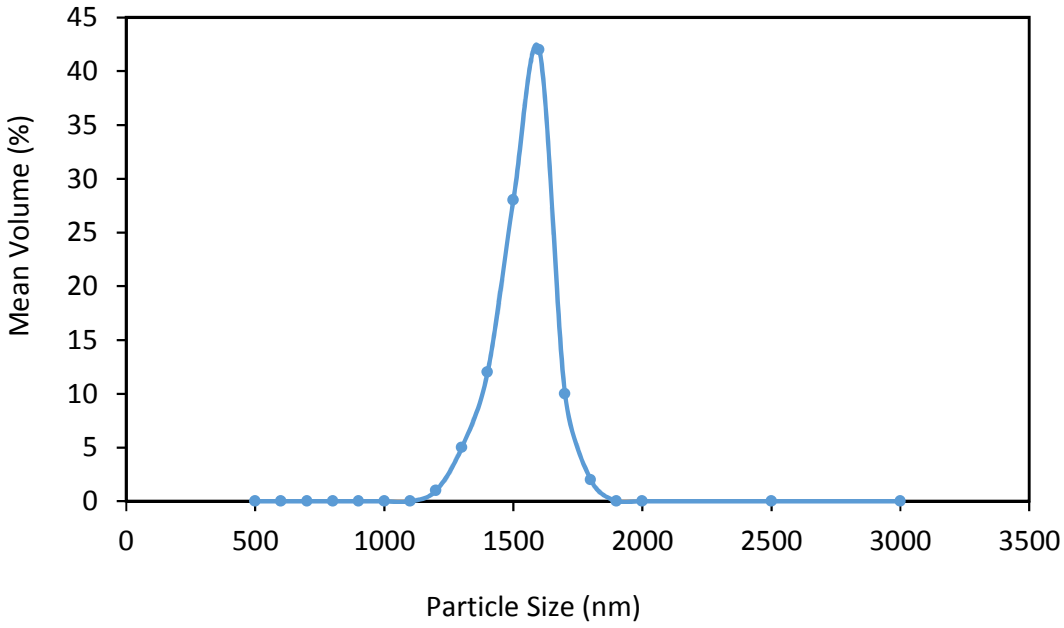

Fig. 7 Particle size distribution of the magnetic silica aerogel nanodispersion using 36% sonication amplitude and 6.2 min sonication time

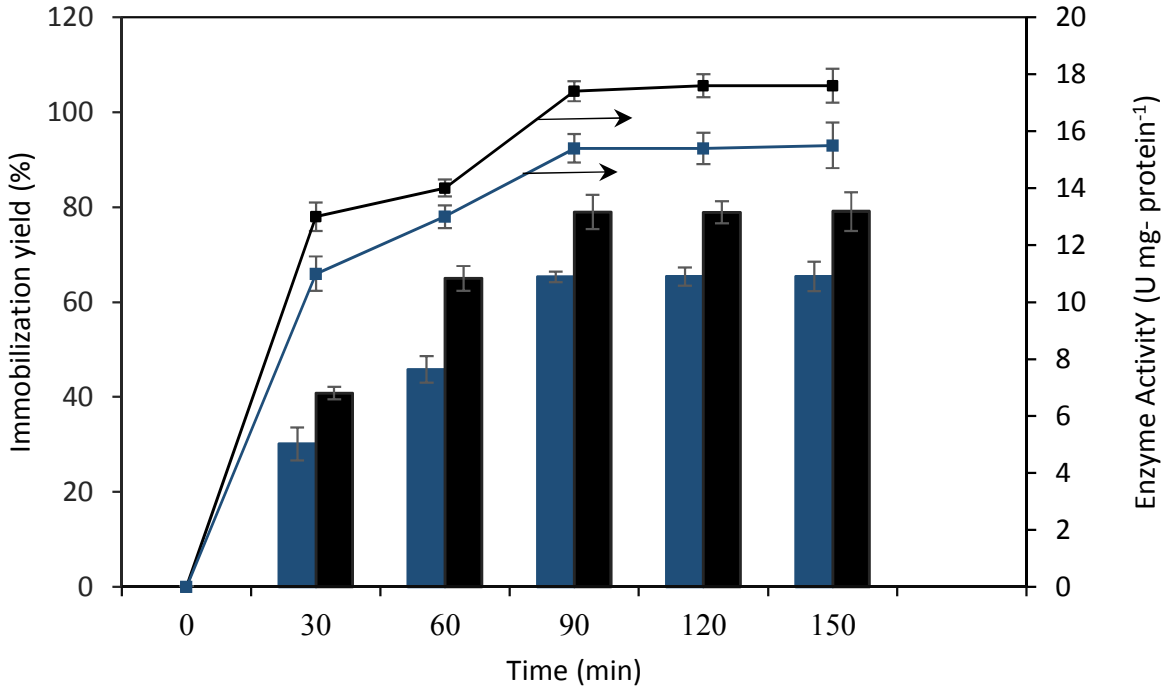

Fig. 8 Comparison between performance of dispersed (■) and non-dispersed (■) supports

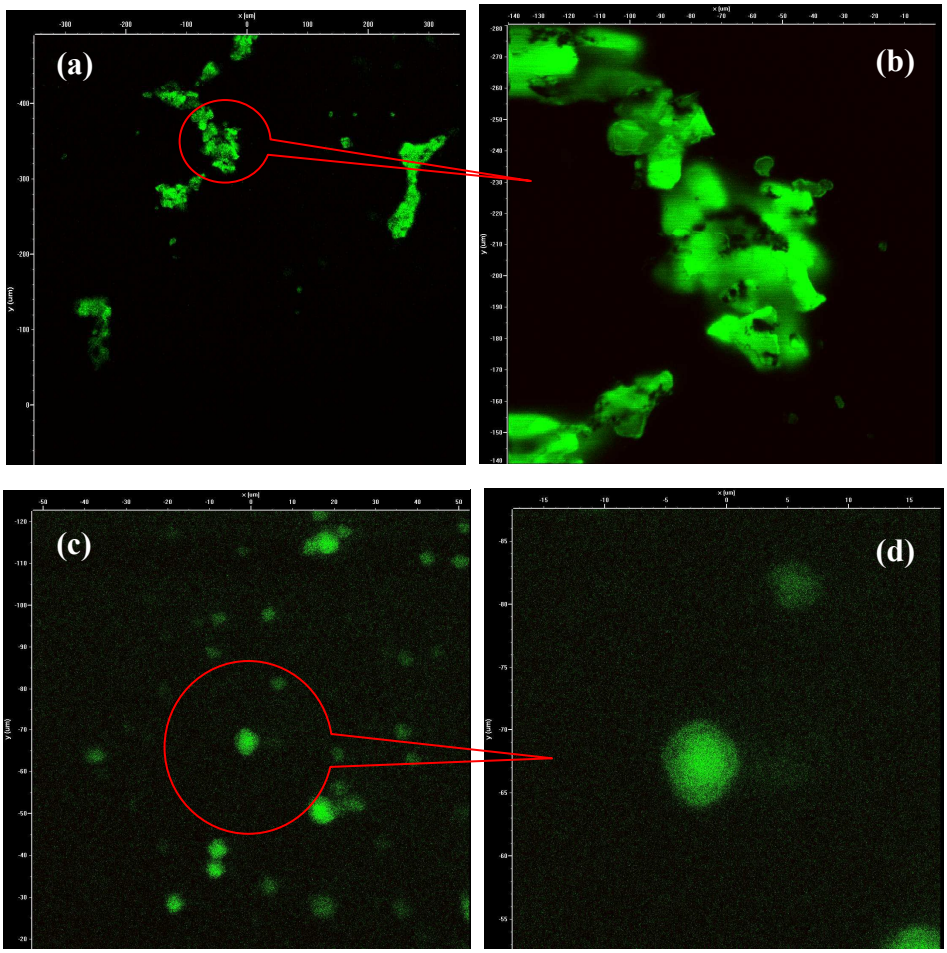

Fig. 9 CLSM images of immobilized FITC-labeled lipase in non-dispersed (a, b) and dispersed (c, d) magnetic silica aerogel at two magnifications.

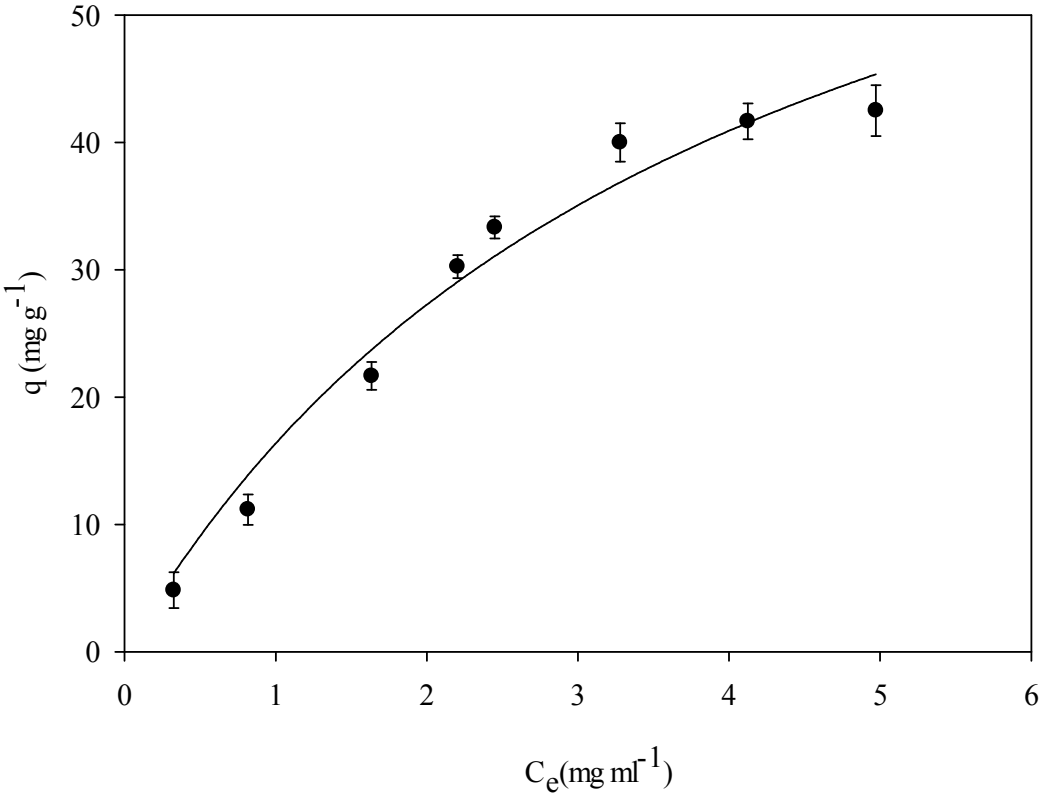

Fig. 10 Adsorption equilibrium of *Candida rugosa* lipase on dispersed magnetic silica aerogel at ambient temperature

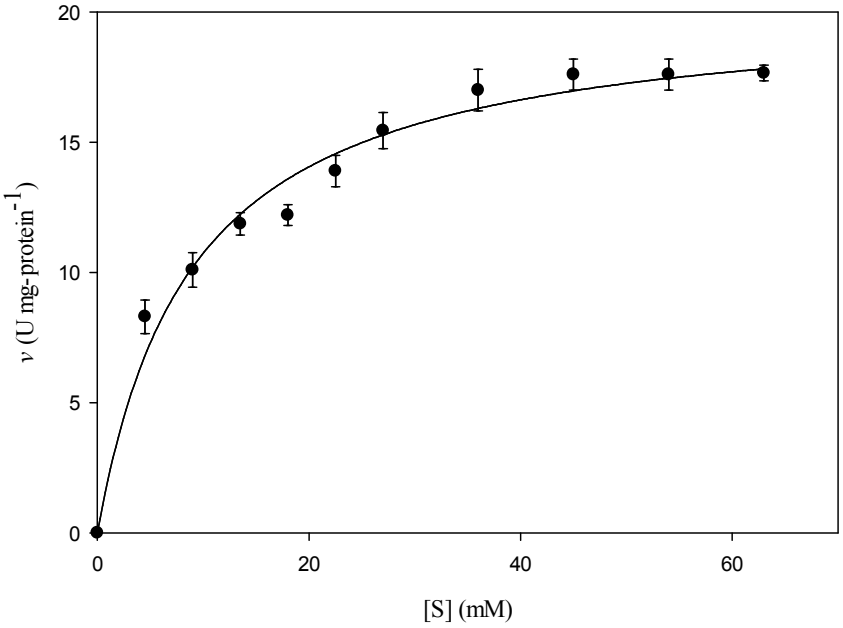

Fig. 11 Michaelis-Menten kinetic curve of dispersed magnetic silica aerogel-lipase

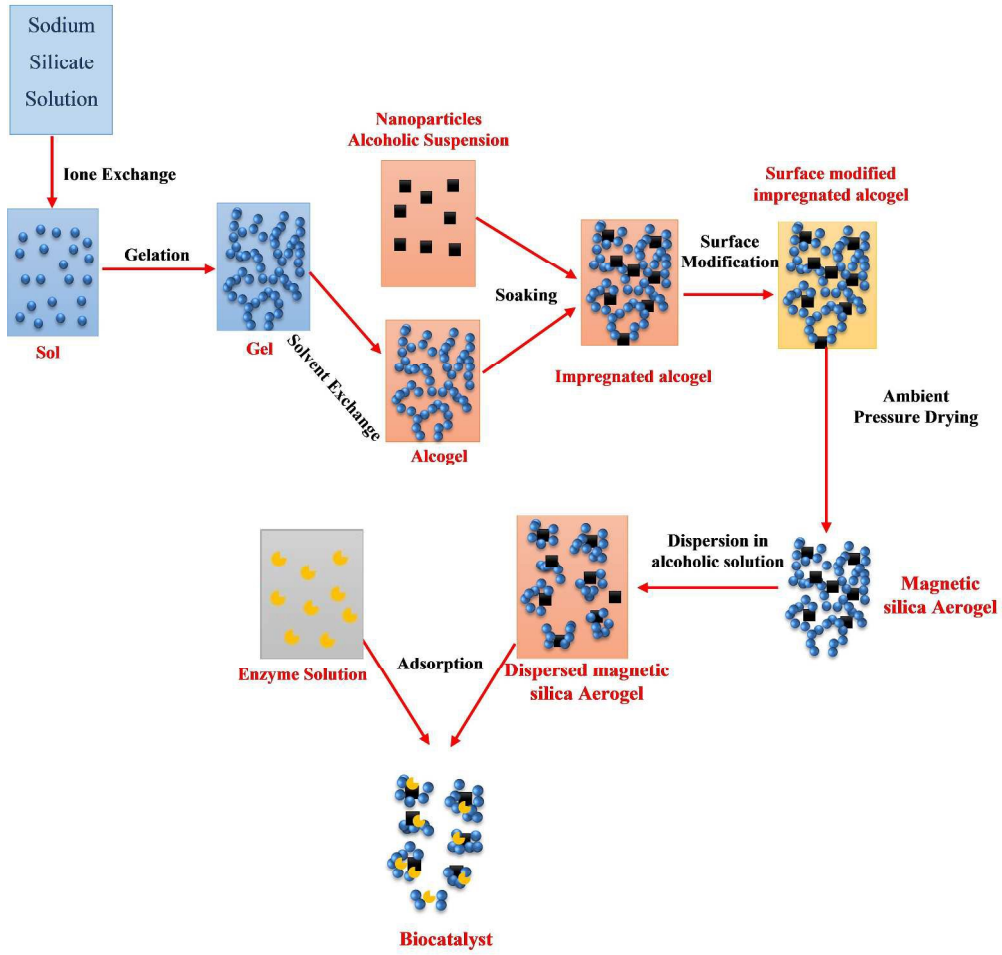

C. rugosa lipase was successfully immobilized on hydrophobic magnetic silica aerogel nanodispersion by simple physical adsorption.

985x1098mm (120 x 120 DPI)